Talanta 233 (2021) 122567

Contents lists available at ScienceDirect

Talanta

journal homepage: www.elsevier.com/locate/talanta

Fabrication of G-quadruplex/porphyrin conjugated gold/persistent luminescence theranostic nanoprobe for imaging-guided photodynamic therapy

Yu-Bin Su [a,b,c], Xu Zhao [a,b,c], Li-Jian Chen [a,b,c], Hai-Long Qian [a,b,c], Xiu-Ping Yan [a,b,c,d,*]

[a] State Key Laboratory of Food Science and Technology, Jiangnan University, Wuxi, 214122, China
[b] International Joint Laboratory on Food Safety, Jiangnan University, Wuxi, 214122, China
[c] Institute of Analytical Food Safety, School of Food Science and Technology, Jiangnan University, Wuxi, 214122, China
[d] Key Laboratory of Synthetic and Biological Colloids, Ministry of Education, School of Chemical and Material Engineering, Jiangnan University, Wuxi, 214122, China

ARTICLE INFO

Keywords:
Photodynamic therapy
Persistent luminescence nanoparticles
Theranostics
Imaging-guided therapy

ABSTRACT

Photodynamic therapy (PDT) received great attention in cancer therapy due to the advantages of negligible drug resistance, low side effects, and minimal invasiveness. Development of theranostic nanoprobes with specific imaging-guided PDT is of great significance in the field. Herein we report the fabrication of a novel theranostic nanoprobe porphyrin/G-quadruplex conjugated gold/persistent luminescence nanocomposites for imaging-guided PDT. The developed nanoprobe contains NIR-emitting persistent luminescent nanoparticles (PLNP) as the core for autofluorescence-free bioimaging and Au coating on PLNP for facile subsequent DNA conjugation. The DNA sequence is designed to contain G-rich AS1411 aptamer for recognizing the over-expressed cellular nucleolin of cancer cell and forming a G-quadruplex structure to combine with tetrakis (4-carboxyphenyl) porphyrin (TCPP) to realize PDT. The AS1411 aptamer-contained DNA conjugated Au-coated PLNP is rapidly prepared *via* a freezing method with high content of DNA and good aqueous stability. Meanwhile, TCPP is easily loaded into the G-quadruplex structure formed from G-rich AS1411 aptamer on the surface of Au/PLNP in presence of K^+. The theranostic nanoprobe gives integrated merits of PLNP for autofluorescence-free bioimging, TCPP for PDT and AS1411 aptamer-contained DNA for specific binding to cancer cells. This work provides a new specially designed imaging-guided PDT nanoplatform for theranostics.

1. Introduction

Photodynamic therapy (PDT) has received great attention in cancer therapy due to the advantages of negligible drug resistance, low side effects, minimal invasiveness, and high site-specific activation [1,2]. As one of the key components of PDT, an ideal candidate photosensitizer (PS) should have the ability for efficient production of reactive oxygen species (ROS) upon light irradiation with high specificity and hydrophilicity but without dark toxicity [3]. Porphyrin and its derivatives are important candidates due to their high photosensitivity, good $^1O_2$ quantum yield and chemical versatility [4]. However, the nonspecificity of the porphyrin may cause the endocytosis of both cancer and normal cells and suffer the risk of side effects. Thus, the hydrophilic porphyrin with good tumor specificity is still extremely needed to achieve high ROS generation efficiency under the light irradiation.

The high specificity makes aptamers be widely applied in diverse fields, including biosensors [5], contrast agents [6], drug delivery [7] and PDT [8]. Compared with protein-based antibodies or enzymes, aptamers are usually chemically stable and can be synthesized with high reproducibility and purity [9]. Besides, G-rich or C-rich aptamers could form the G-quadruplex or I-motif structures under certain conditions [10,11]. The G-quadruplex or I-motif contained aptamers could accept a desired organic molecule to give new properties, such as G-quadruplex/porphyrin, which could be applied to PDT [12]. However, simple DNA sequences always suffer from enzymolysis in complex physiological environments, leading to the premature release and loss of drugs and low therapeutic effect. To address this issue, tight packing of DNA on the nanomaterial surface or stable formation of DNA is a good choice to resist enzymolysis [8].

Various kinds of nanomaterials, such as quantum dot (QD) [13],

* Corresponding author. State Key Laboratory of Food Science and Technology, Jiangnan University, Wuxi, 214122, China.
E-mail address: xpyan@jiangnan.edu.cn (X.-P. Yan).

https://doi.org/10.1016/j.talanta.2021.122567
Received 28 February 2021; Received in revised form 24 May 2021; Accepted 26 May 2021
Available online 1 June 2021

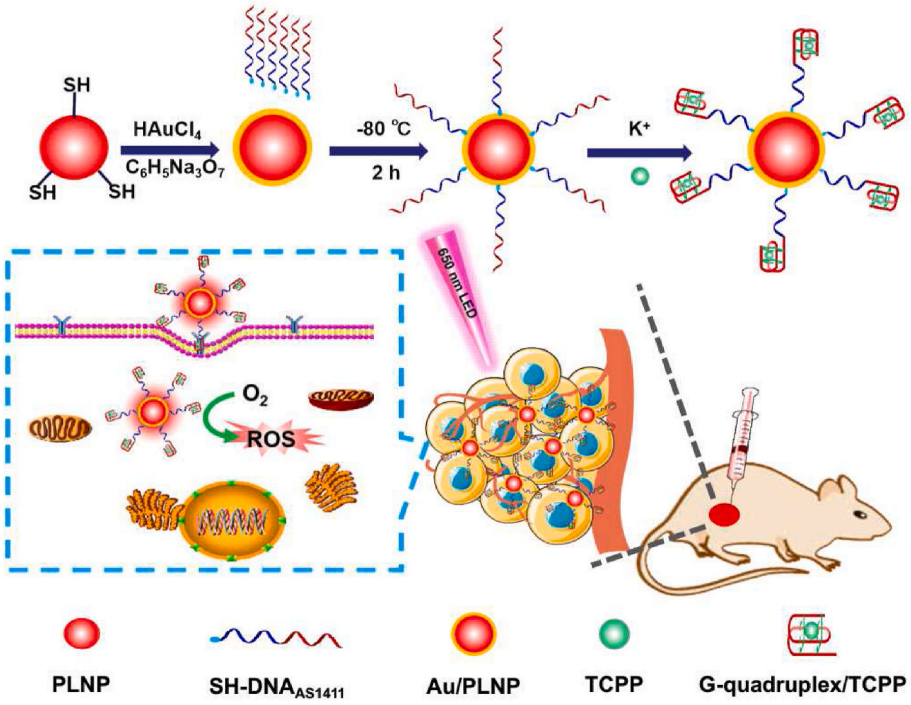

Scheme 1. Schematic illustration of the preparation of the theranostic nanprobe TCPP-GDNA-Au/PLNP for PDT.

graphene oxide (GO) [14], gold nanoparticle (AuNPs) [15], metallic oxide [16], polymeric nanoparticles [17] and persistent luminescence nanoparticles (PLNP) [18], have been conjugated with DNA for diverse applications. Meanwhile, DNA conjugation also improves the dispersity and biocompatibility of nanomaterials. PLNP have attracted considerable attention because of their unique ability to emit long-lasting luminescence after excitation stops [19–22]. Particularly, the near-infrared (NIR)-emitting PLNP are ideal candidate phosphors in bioimaging and cancer treatment application without the tissue autofluorescence interference [23–26]. As we know, the functionalization of the PLNP is essential for biological applications. Unfortunately, it is not easy to conjugate other chemical or biomedical agents onto the surface of PLNP. Surface functionalization of PLNP was usually achieved *via* coating with siloxanes, such as tetraethoxysilane [27], (3-aminopropyl)-triethoxysilane [25,26,28], (3-iodopropyl)-trimthoxysilane [29] and 3-mercaptopropionic acid [30]. However, the functional groups grafted on the surface of PLNP *via* such coating strategies with siloxane derivatives are limited, leading to low functionalization. Therefore, a simple and biocompatible protocol is still extremely needed to broaden the strategies for bridging PLNP in biological applications. Au coating on PLNP is attractive for further surface modification with thiolated chemical or biomedical agents through Au–S bond without the need for extra reagents [30,31]. Recent study showed that the thiolated DNA could be rapidly conjugated with AuNPs *via* freezing with high DNA density without extra reagents [32].

Herein, we report the fabrication of porphyrin/G-quadruplex DNA conjugated gold/persistent luminescence nanocomposites for PDT (Scheme 1). $Zn_{1.25}Ga_{1.5}Ge_{0.25}O_4$:0.5%$Cr^{3+}$,2.5%$Yb^{3+}$,0.25%$Er^{3+}$ PLNP is used as the core of the nanocomposites due to its long lasting NIR emission [33,34]. Au is coated on the surface of PLNP (Au/PLNP) for facile subsequent DNA conjugation (DNA-Au/PLNP) *via* freezing method without extra reagent. The DNA sequence is designed to contain a G-rich AS1411 aptamer for not only recognizing the over-expressed cellular nucleolin of cancer cell but also forming a G-quadruplex structure (GDNA) in the presence of K^+ to combine with the PS tetrakis (4-carboxyphenyl) porphyrin (TCPP) to realize PDT. The as-prepared TCPP/G-quadruplex-Au/PLNP (TCPP-GDNA-Au/PLNP) is promising as a novel theranostic nanoprobe for efficient persistent luminescence imaging-guided PDT.

2. Materials and methods

2.1. Materials and chemicals

The DNA containing G-rich AS1411 (5′-(GGTGGTGGTGGTTGTGGTG GTGGTGGCCCAGGTGACTG–C_6SH)–3′) and its complementary DNA labeled with Cy5.5 (5′Cy5.5-CAGT-CACCTGGGGGAGTATTGCGGAGGAAGGT-3′) were synthesized by Shanghai Sangon Biotechnology Co. Ltd. (Shanghai, China). (3-Mercaptopropyl)trimethaxysilane, TCPP and $HAuCl_4$ were obtained from Energy Chemical Co. Ltd. (Shanghai, China). $Zn(NO_3)_2{\cdot}6H_2O$, Ga_2O_3, GeO_2, $Cr(NO_3)_3{\cdot}9H_2O$, $Yb(NO_3)_3$, Er_2O_3, KCl, tris(hydroxymethyl)aminomethane (Tris), dimethyl sulfoxide (DMSO), and dimethylformamide (DMF) came from Sinopharm Group Co. Ltd. (Beijing, China). Hexadecyl trimethyl ammonium bromide (CTAB), 3-(4,5-dimethylthiazol-2-yl)-2,5-diphenyltetrazolium bromide (MTT), 2′,7′-dichlorofluorescein diacetate (DCFH-DA), glutathione (GSH) and trisodium citrate were provided by Aladdin Co. Ltd. (Shanghai, China). Propidium iodide (PI) and 9,10-anthracenediyl-bis(methylene)dimalonic acid (ABDA) provided by Macklin Co. Ltd. (Shanghai, China). Ultrapure water (Wahaha Group Co. Ltd, Hangzhou, China) was used throughout. All chemicals used were of analytical grade as received without further purification.

2.2. Preparation of PLNP-SH

The PLNP ($Zn_{1.25}Ga_{1.5}Ge_{0.25}O_4$:0.5%Cr, 2.5%Yb, 0.25%Er) and hydroxyl-functional PLNP (PLNP-OH) were prepared according to our previous work [33,34]. 50 mg of PLNP-OH was dispersed in 20 mL of DMF under sonication, and then 200 μL of (3-mercaptopropyl)trimethaxysilane was added under vigorous stirring at 80 °C for 24 h. The resulting thiol-functional PLNP (PLNP-SH) was collected by centrifugation at 10,000 rpm for 15 min, and washed with DMF three times. The final PLNP-SH powder was obtained by freeze-drying to keep its good dispersibility and avoid oxidating for further use.

2.3. Preparation of Au/PLNP

2 mL different concentrations of $HAuCl_4$ (0.005%, 0.01%, 0.05% and 0.1% w/v) were mixed with 2 mL PLNP-SH (1 mg mL^{-1}) aqueous solution under ultrasonic, respectively. After 5 min, 1.2 mL trisodium citrate (20 mM) was added dropwise to the mixture under ultrasonication and the color of the solution changed from purple to red. After ultrasonication for 20 min and the color of the solution changed negligibly, the red Au/PLNP was collected by centrifugation at 10,000 rpm for 15 min and washed with ultrapure water three times to remove unreacted $HAuCl_4$ and trisodium citrate. The red Au/PLNP powder was obtained by freeze-drying for further use.

2.4. Preparation of DNA-Au/PLNP

DNA-Au/PLNP was prepared by a freezing method [32]. Briefly, 25 μL DNA (30 μM) was mixed with 2.2 mL Au/PLNP (0.5 mg mL^{-1}) aqueous solution. The mixture was then placed in a laboratory freezer at −80 °C for 2 h, followed by thawing at room temperature. After thawing, 250 μL 3 M NaCl (final concentration = 300 mM) was added to the above mixture immediately to maintain a high salt concentration. The free DNA was removed after thawing by centrifugation and washing. Then, the DNA-Au/PLNP was redispersed in Tris-HCl buffer (pH 7.5, 0.1 M KCl).

2.5. Preparation of GDNA-Au/PLNP and TCPP-GDNA-Au/PLNP

20 μL DMSO was added to 2 mL of 0.5 mg mL^{-1} DNA-Au/PLNP in Tris-HCl buffer (pH 7.5, 0.1 M KCl) to make the 1% wt final concentration of DMSO. The prepared DNA-Au/PLNP solution in 1% wt DMSO was heated to 95 °C for 5 min and naturally cooled to room temperature to form G-quadruplex DNA-Au/PLNP (GDNA-Au/PLNP). 200 μL TCPP (100 μM) was subsequently added to the above prepared GDNA-Au/PLNP solution and shaken for 12 h. The free TCPP was removed by centrifugation and washed with Tris-HCl buffer three times. Finally, the resulting TCPP-GDNA-Au/PLNP was redispersed in Tris-HCl buffer (pH 7.5, 0.1 M KCl) and stored at 4 °C for further use.

2.6. Singlet oxygen generation in solution

Briefly, 2 mL of 500 μg mL^{-1} Au/PLNP, DNA-Au/PLNP and TCPP-GDNA-Au/PLNP solution were respectively mixed with a certain concentration of ABDA (final concentration was 50 μM). The mixture was set in dark and irradiated with a 650 nm LED light (0.2 W cm^{-2}) for 0, 2, 4, 6, 8, 10, 14, 18 and 20 min for UV–vis tests, respectively.

2.7. Detection of intracellular singlet oxygen

DCFH-DA was used to monitor singlet oxygen generation in vivo. In brief, HeLa cells were incubated with Au/PLNP, DNA-Au/PLNP and TCPP-GDNA-Au/PLNP (500 μg mL^{-1}) respectively for 24 h. Then, the fresh medium containing 20 μM DCFH-DA was added to HeLa cells after washing with PBS twice. After further incubation for 30 min, the cells were washed with PBS twice and irradiated by 650 nm LED (0.2 W cm^{-2}, 20 min), and the fluorescence images of the cells were taken by confocal laser scanning microscopy (CLSM) immediately. The fluorescence of DCFH-DA was collected within 550–650 nm under excitation at 488 nm.

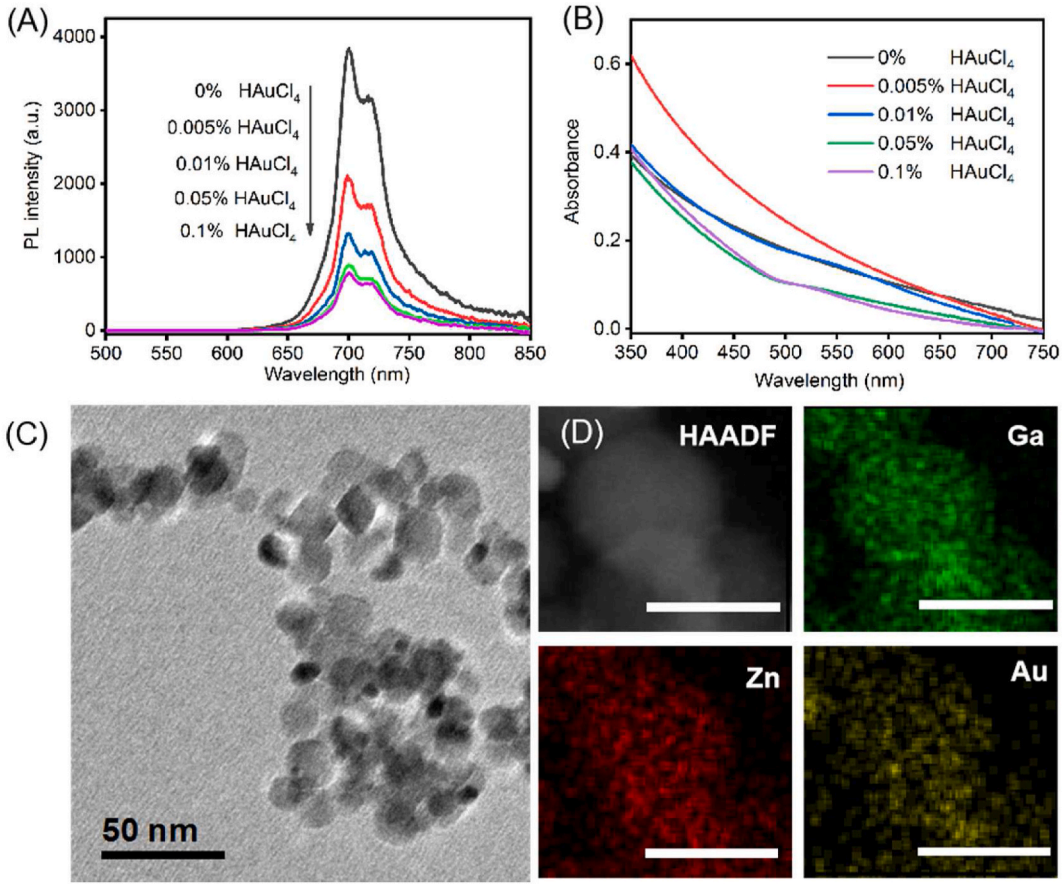

Fig. 1. (A) Persistent luminescence spectra and (B) UV–Vis absorption spectra of Au/PLNP solution (0.5 mg mL^{-1}) prepared with different concentrations of $HAuCl_4$ (0%, 0.005%, 0.01%, 0.05% and 0.1% w/v). (C) TEM images of Au/PLNP, (D) HAADF-STEM-EDX mapping of Au/PLNP, scale bar is 20 nm.

2.8. Cell apoptosis assay

PI was used to monitor cell apoptosis. Briefly, HeLa cells were incubated with Au/PLNP, DNA-Au/PLNP and TCPP-GDNA-Au/PLNP (500 μg mL^{-1}) respectively for 12 h and then irradiated with 650 nm LED (0.2 W cm^{-2}) for 20 min. After incubation for further 12 h, the fresh medium containing 100 μg mL^{-1} PI was added to HeLa cells after washing with PBS twice and incubation for 10 min. After that, the medium containing 100 μg mL^{-1} PI was removed while the cells were washed with PBS. Finally, the fluorescence images of the cells were taken by a CLSM. The fluorescence of PI was collected within 550–650 nm under excitation at 561 nm.

2.9. Animal experiments

The nude mice (5 week-old BALB/c female) were provided by Shanghai Slac Laboratory Animal Technology (Shanghai, China). Animal procedures were performed according to the guidelines of the Ethics Committee of Jiangnan University for animal experiments (JN. No20200710n0200910 [145]). All mice were housed in SPF-level animal rooms (26 °C, a humidity of 50%) and free to obtain sterile food and water. Tumor-bearing BALB/c female nude mice were prepared by subcutaneous implanting with HeLa cells. The tumor-bearing mice were randomly divided into five groups (n = 5) when the tumor volume was about 200 mm^3. DNA-Au/PLNP, TCPP-GDNA-Au/PLNP (4.0 mg mL^{-1}, 100 μL) and saline as control were orthotopically injected into tumor-bearing mice, respectively. The tumor sites of mice in the groups of DNA-Au/PLNP and TCPP-GDNA-Au/PLNP were irradiated with 650 nm LED light (0.2 W cm^{-2}, 20 min) at 6 h postinjection. The weight of mice and sizes of tumors were measured every other day. Tumor volumes were calculated by the following equation: 1/2 × length × $(width)^2$ (where the length and the width indicate the longest and the shortest diameters (mm) of the tumor, respectively) [43]. The relative tumor volume was defined as V/V_0 (where V_0 is the original tumor volume before treatment). After 14 days of treatment, tumor-bearing mice were euthanized. Then, tumor tissue were dissected and treated with 4% w/v paraformaldehyde and stored at 4 °C.

2.10. Histology examination

H&E staining assay of the sliced tissues was performed according to the manufacturer's protocol and the stained tissue sections were observed under the microscope.

3. Results and discussion

3.1. Preparation and characterization of PLNP, PLNP-OH, PLNP-SH and Au/PLNP

The PLNP and PLNP-OH were synthesized according to our previous work [33,34]. The as-prepared PLNP is generally spherical with the size of 15.0 ± 2.5 nm (measured from 100 randomly chosen nanoparticles) (Fig. S1A and Fig. S2). The excitation and emission spectra (Fig. S1B), and the X-ray diffraction (XRD) pattern (Fig. S1C) of the as-prepared PLNP are in good agreement with those reported previously [19,23,25,33]. In addition, the as-prepared PLNP exhibits long-lasting luminescence after the UV lamp irradiation stopping and can be reactivated with a 650 ± 10 nm LED light irradiation (Fig. S1D and Fig. S3). These results indicate that the NIR-emitting PLNP has great potential for bioimaging without the tissue autofluorescence interference.

PLNP-SH was prepared from PLNP-OH and (3-mercaptopropyl)trimethaxysilane for further preparation of gold coated PLNP (Au/PLNP). Successful preparation of PLNP-SH was confirmed by the appearance of -SH and Si–O band at 2370 cm^{-1} and 1114 cm^{-1} in FT-IR spectra, respectively (Fig. S4A) [25], the change of zeta-potential from positive to negative (Fig. S4B) and the increase of hydrodynamic diameter

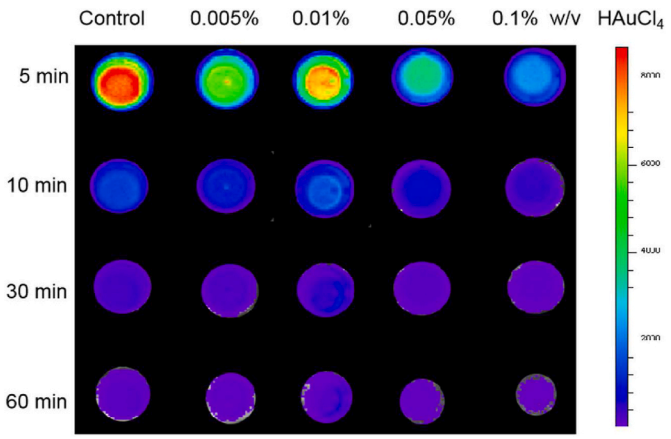

Fig. 2. Persistent luminescence images of the Au/PLNP solution (1 mg mL^{-1}) prepared with different concentrations of $HAuCl_4$.

(Fig. S4C). For the preparation of Au/PLNP, Au^{3+} was chelated with the terminal –SH group of PLNP-SH and reduced to Au^0 on the surface of PLNP by trisodium citrate under ultrasonication. However, the luminescence of PLNP decreased as the concentration of the $HAuCl_4$ increased (Fig. 1A), indicating that Au coating led to the luminescence quenching of PLNP. For this reason, the concentration of $HAuCl_4$ was optimized to obtain Au/PLNP with minimum luminescence quenching. The appearance of the characteristic absorption peak of AuNPs at 550 nm up to 0.01% (w/v) $HAuCl_4$ (Fig. 1B) and the change of the solution color from white to red (Fig. S5) indicate the successful Au coating onto the surface of PLNP-SH. Meanwhile, 0.01% (w/v) $HAuCl_4$ still gave obvious luminescence of Au/PLNP after the irradiation with a 650-nm LED light for 5 min (Fig. 2). Therefore, 0.01% (w/v) $HAuCl_4$ was chosen to prepare Au/PLNP for further characterization and application. Fig. 1C shows that the as-prepared Au/PLNP was monodisperse and roughly spherical with the size of 15.0 ± 5.0 nm (determined from 100 randomly chosen nanoparticles, Figure S6A). HAADF-STEM-EDX mapping and energy dispersive X-ray spectroscopy (EDS) revealed the Au coating on the surface of PLNP and the thickness of Au shell was about 1.1 nm (Fig. 1D and Fig. S6B).

3.2. Conjugation of DNA with Au/PLNP

AS1411 aptamer (a G-rich DNA aptamer) which is specific to most cancer cellular nucleolin was used for cancer cell targeting. The G-rich DNA aptamer enables the formation of G-quadruplex to combine with porphyrin molecule for PDT [12]. However, direct conjugation of AS1411 aptamer on to Au/PLNP makes it difficult to form G-quadruplex due to the steric affect [35]. For this reason, an additional DNA linker (CCCAGGTGACTG) was attached to the G-rich AS1411 aptamer to form the AS1411 aptamer contained DNA structure not only to keep the ability for cancer cell targeting, but also to facilitate the formation of a G-quadruplex structure in the presence of K^+ to combine with the TCPP to realize PDT. So, the concentration of the AS1411 aptamer contained DNA was optimized to improve the specific binding to cancer cell and the amount of porphyrin molecule combined with AS1411. For this purpose, the Cy5.5 labeled linker complementary DNA was hybridized with AS1411 aptamer to quench the luminescence of Au/PLNP. The luminescence intensity of Au/PLNP (0.5 mg mL^{-1}) decreased as the concentration of the complementary DNA increased up to 0.3 μM, then levelled off with further increase of the concentration of the complementary DNA (Fig. S7). Therefore, 0.3 μM of the AS1411 aptamer contained DNA was used to conjugate with Au/PLNP (0.5 mg mL^{-1}).

DNA-Au/PLNP gave more negative zeta potential than Au/PLNP due to the phosphate on the DNA (Fig. 3A). Moreover, DNA conjugation made the absorption peak of Au/PLNP red-shift from 530 nm to 535 nm

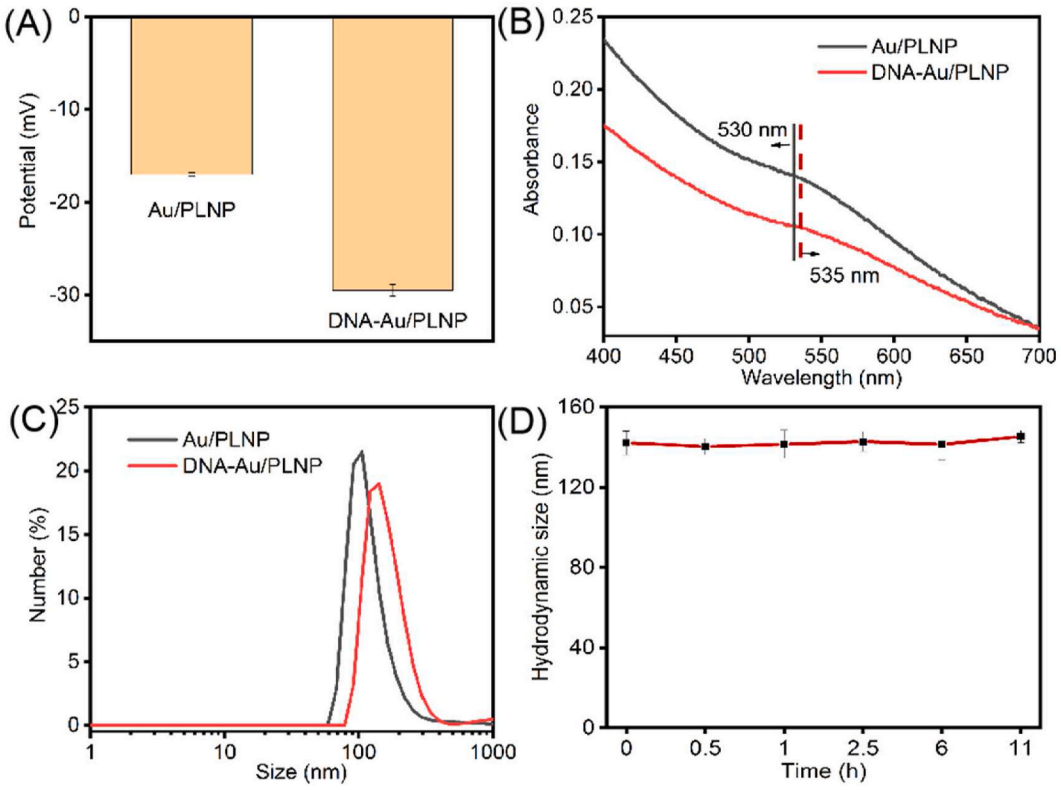

Fig. 3. (A) Zeta potential and (B) UV–vis absorption spectra of the prepared Au/PLNP and DNA-Au/PLNP in aqueous solution (0.5 mg mL^{-1}). (C) Hydrodynamic size distribution of the prepared Au/PLNP and DNA-Au/PLNP. (D) Change of the hydrodynamic size of the DNA-Au/PLNP dispersed in aqueous solution (0.5 mg mL^{-1}) with time.

(Fig. 3B) [36], the dynamic diameter of the nanocomposite increase from 105.7 nm to 141.8 nm (Fig. 3C), the bands at 3500-3300 cm^{-1} and 1636 cm^{-1} the $–NH_2$ and C–O groups of DNA increase (Fig. S8) [37,38]. These results demonstrate that the DNA was successfully conjugated with Au/PLNP.

The as-prepared DNA-Au/PLNP showed excellent stability in aqueous solution due to the insignificant change of the dynamic diameter in 11 h (Fig. 3D). Besides, no significant change in the dynamic diameter of DNA-Au/PLNP with the concentration of GSH was observed (Fig. S9), indicating that the as-prepared DNA-Au/PLNP was stable in varying concentrations of GSH (5 mM–20 mM). Furthermore, the amounts of DNA conjugated with Au/PLNP were determined by UV–vis spectroscopy for the comparison of the freezing method with two other methods, salt-aging and low-pH, which are often used to conjugate DNA and AuNP [39,40]. The freezing method gave the largest amounts of DNA conjugated onto Au/PLNP than the two other methods (Fig. S10). The high DNA loading also explains the excellent colloidal stability of the DNA conjugated Au/PLNP. This result reveals that the freezing method is an ideal method for simple and rapid conjugating of DNA and Au/PLNP.

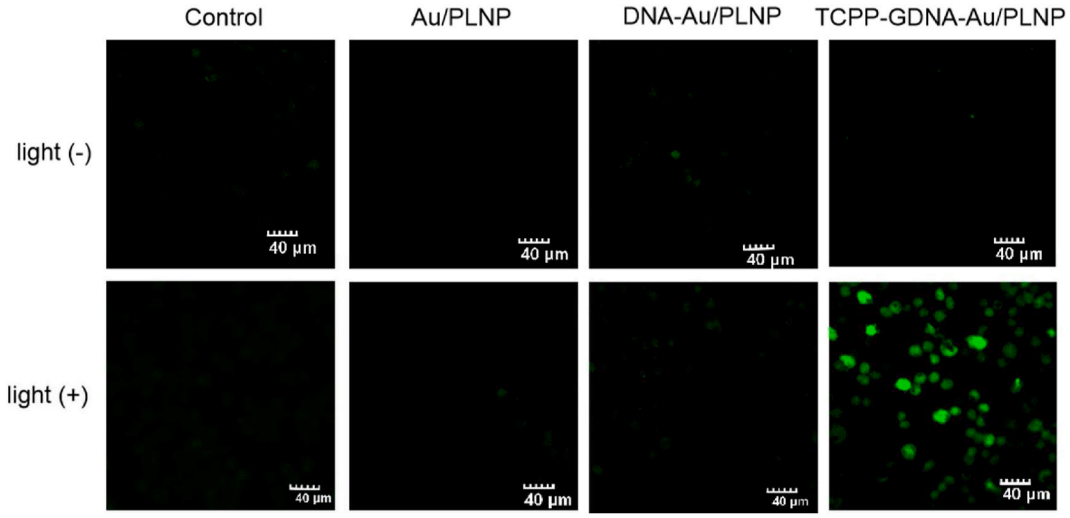

Fig. 4. Detection of the intracellular singlet oxygen generation: CLSM images of HeLa cells incubated with Au/PLNP, DNA-Au/PLNP and TCPP-GDNA-Au/PLNP with or without 650 nm LED irradiation, respectively. HeLa cells were stained with DCFH-DA as the intracellular singlet oxygen probe.

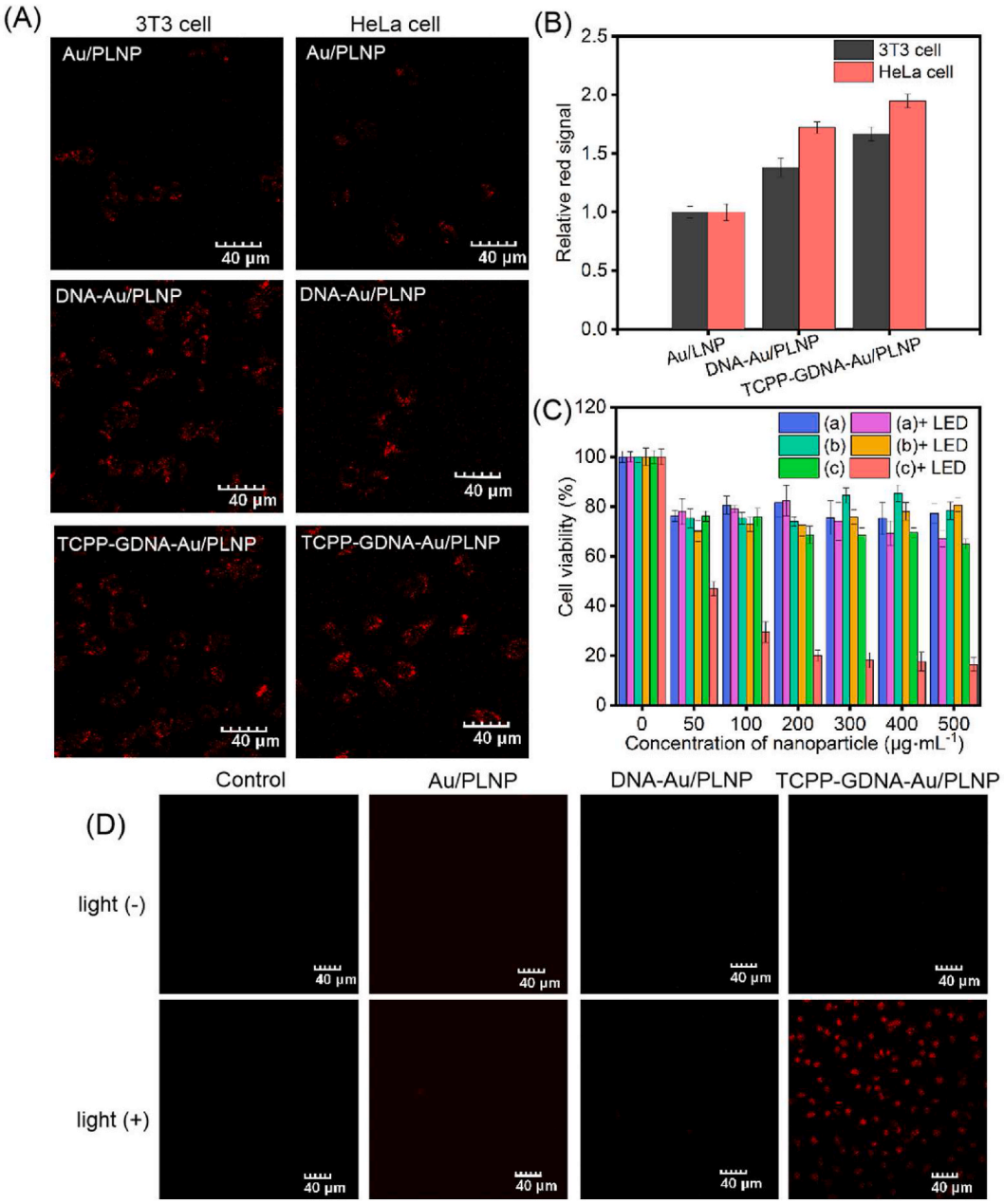

Fig. 5. (A) CLSM images of the HeLa and 3T3 cells treated with Au/PLNP, DNA-Au/PLNP and TCPP-GDNA-Au/PLNP. (B) Relative luminescence intensity of the HeLa and 3T3 cells treated with Au/PLNP, DNA-Au/PLNP and TCPP-GDNA-Au/PLNP (The detailed red signal intensity was calculated by Image J software with the same amount of cells and the luminescence intensity of the cells treated with Au/PLNP was taken as 1). (C) Cell viability of the HeLa treated with Au/PLNP (a), DNA-Au/PLNP (b) and TCPP-GDNA-Au/PLNP (c) with or without 650 nm LED irradiation. (D) CLSM images of HeLa cells incubated with Au/PLNP, DNA-Au/PLNP and TCPP-GDNA-Au/PLNP with or without 650 nm LED irradiation. HeLa cell was stained by PI to evaluate cell viability. (For interpretation of the references to color in this figure legend, the reader is referred to the Web version of this article.)

3.3. Formation and singlet oxygen generation of TCPP-GDNA-Au/PLNP

The DNA conjugated Au/PLNP could form a G-quadruplex structure (GDNA-Au/PLNP) in the presence of K^+ owing to the G-rich aptamer AS1411 [10,11], which could accept the TCPP to form TCPP-GDNA-Au/PLNP [12]. Here, excessive K^+ (0.1 M) was used to form and stabilize the G-quadruplexes structure as it strongly interacted with guanine base owing to the negative electrostatic potential of guanine base [10,11]. Meanwhile, the TCPP was embeded into G-quadruplex structure to form TCPP-GDNA-Au/PLNP [12]. The G-quadruplex conformation of DNA contained aptamer AS1411 was confirmed by circular dichroism (CD) spectroscopy (Fig. S11). The minimum peak at 238 nm in combination with the maximum peak at 263 nm confirms that the aptamer AS1411contianed DNA indeed formed a stable parallel-stranded G-quadruplex structure in presence of K^+ [10].

The singlet oxygen generation ability of TCPP-GDNA-Au/PLNP was measured in aqueous solution by UV–vis absorption spectrometry with ABDA as the singlet oxygen probe. TCPP-GDNA-Au/PLNP exhibited fast singlet oxygen generation under the 650 nm LED irradiation due to the presence of TCPP with highly efficient light-induced ROS generation under the 650 nm LED irradiation [41] (Fig. S12). In addition, we investigated that the effect of the concentration of AS1411 aptamers on the amount of TCPP linked to nanoparticle and the ROS yield of the nanoprobe. The TCPP-GDNA-Au/PLNP conjugated with more AS1411 aptamers exhibited faster singlet oxygen generation under the 650 nm LED irradiation (Fig. S13), indicating that the concentration of AS1411

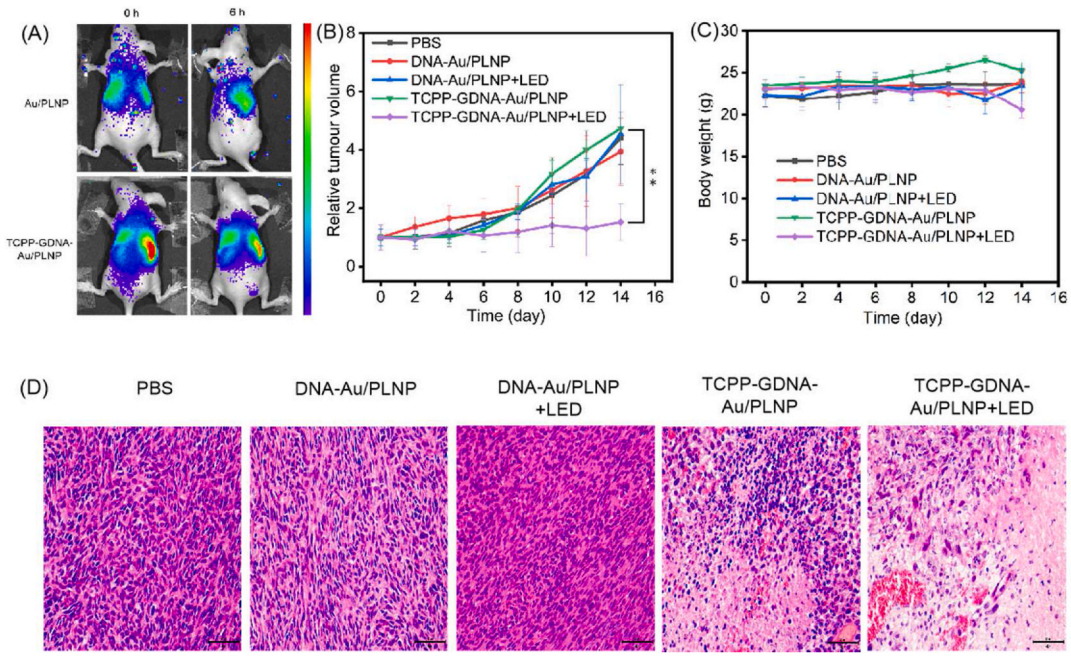

Fig. 6. (A) Persistent luminescence image of HeLa tumor-bearing BALB/c-nude mice by tail veil injection with Au/PLNP and TCPP-GDNA-Au/PLNP. (B) Tumor growth curve (Asterisks denote statistically significant: $^{**}P < 0.01$) and (C) time dependent body weight of nude mice bearing HeLa tumors after treatment with PBS, DNA-Au/PLNP, DNA-Au/PLNP with 20 min irradiation by 650 nm LED light (0.2 W cm^{-2}), TCPP-GDNA-Au/PLNP, TCPP-GDNA-Au/PLNP with 20 min irradiation by 650 nm LED light (0.2 W cm^{-2}), respectively. (D) Histological analysis of tumors tissues with H&E staining (scale bar is 50 μm).

aptamers affected the amount of TCPP linked to nanoparticle and the ROS yield of the nanoprobes.

DCFH-DA was employed to investigate the intracellular singlet oxygen generation of TCPP-GDNA-Au/PLNP by CLSM [42]. CLSM images of HeLa cells treated with Au/PLNP, DNA-Au/PLNP and TCPP-GDNA-Au/PLNP were compared in Fig. 4. TCPP-GDNA-Au/PLNP treatment gave significantly brighter green fluorescence than the treatment with Au/PLNP, DNA-Au/PLNP under the 650 nm LED irradiation for 20 min, while the fluorescence of HeLa cells in all of the groups was negligible without the 650 nm LED irradiation. These results indicate that TCPP-GDNA-Au/PLNP can catalyze the O_2 in living cell to form singlet oxygen under the 650 nm LED irradiation.

3.4. Cancer cell targeting of TCPP-GDNA-Au/PLNP

The ability of TCPP-GDNA-Au/PLNP for cancer cell targeting was investigated by comparing the internalization efficiencies of normal cell (3T3) and cancer cell (HeLa) for Au/PLNP, DNA-Au/PLNP and TCPP-GDNA-Au/PLNP. CLSM images show that both DNA-Au/PLNP-treated and TCPP-GDNA-Au/PLNP-treated HeLa cells gave brighter fluorescence than Au/PLNP-treated HeLa cells upon excitation at 561 nm due to the high affinity and specificity of AS1411 aptamer on the surface of Au/PLNP to the over-expressed cellular nucleolin in cancer cells. Meanwhile, TCPP-GDNA-Au/PLNP-treated HeLa cells also showed brighter fluorescence than DNA-Au/PLNP-treated HeLa cells, proving that the G-quadruplex/TCPP on the surface of Au/PLNP remained intact in cancer cells (Fig. 5A and B). Similar trends were seen in the images of 3T3 cells, but cancer cells showed brighter luminescence than the same amount of 3T3 cells (Fig. 5A and B) because of the recognition of AS1411 aptamer for the over-expressed cellular nucleolin in cancer cells. The above results suggest that the DNA-Au/PLNP can bind specifically to cancer cells and the structure of G-quadruplex/TCPP was unaffected in cancer cells.

3.5. Toxicity and PDT effect of TCPP-GDNA-Au/PLNP

The dark toxicity of TCPP-GDNA-Au/PLNP was evaluated by a standard MTT assay on HeLa cells. The viability of HeLa cells incubated with Au/PLNP and DNA-Au/PLNP was more than 70% no matter in the dark or under 650 nm irradiation, indicating that the negligible toxicity of both Au/PLNP and DNA-Au/PLNP up to 500 μg mL^{-1}. In contrast, the viability of HeLa cells treated with 500 μg mL^{-1} TCPP-GDNA-Au/PLNP under 650 nm irradiation (16.4%) was much lower than that in the dark (64.9%) (Fig. 5C). These results indicate that TCPP-GDNA-Au/PLNP possesses excellent phototoxicity for PDT.

The PDT efficiency of TCPP-GDNA-Au/PLNP was further demonstrated by a PI assay. Much brighter red fluorescence was observed in the HeLa cells' nucleus treated with TCPP-GDNA-Au/PLNP after irradiation with the 650 nm LED than in HeLa cells' nucleus treated with Au/PLNP and DNA-Au/PLNP (Fig. 5D). Meanwhile, red fluorescence was not observed in all groups without the 650 nm LED irradiation. These results also show that TCPP-GDNA-Au/PLNP gave strong phototoxicity to kill cancer cells.

3.6. TCPP-GDNA-Au/PLNP for in vivo autofluorescence-free imaging and PDT

The feasibility of TCPP-GDNA-Au/PLNP for autofluorescence-free imaging in vivo was demonstrated through tail veil and intratumor injecting of TCPP-GDNA-Au/PLNP into HeLa tumor-bearing mice. The luminescence signal of TCPP-GDNA-Au/PLNP treated with tail veil injection appeared at the tumor site without tissue autofluorescence interference after 6 h, whereas no obvious luminescence signal of Au/PLNP appeared at the tumor site (Fig. 6A), indicating that TCPP-GDNA-Au/PLNP can be used for imaging guided PDT in vivo. Moreover, the luminescence signal of TCPP-GDNA-Au/PLNP treated with intratumor injection appeared at the tumor site and could retain in the tumor for 20 h (Fig. S14), indicating that intratumorally injected with TCPP-GDNA-Au/PLNP was a candidate for further PDT in vivo to achieve highly effective of PDT. Furthermore, the PDT effect and in vivo tumor growth inhibition of TCPP-GDNA-Au/PLNP were investigated with HeLa tumor-bearing mice to evaluate the anticancer potentials. The mice bearing subcutaneous HeLa tumor (tumor size, ~200 mm^3) were randomly divided into five groups, and intratumorally injected with various

reagents: PBS, DNA-Au/PLNP without light irradiation (light-), DNA-Au/PLNP under 650 nm LED light irradiation (light+), TCPP-GDNA-Au/PLNP without light irradiation (light-) and TCPP-GDNA-Au/PLNP under 650 nm LED light irradiation (light+). The groups of PBS and DNA-Au/PLNP, the tumor sizes of the mice injected with TCPP-GDNA-Au/PLNP after 650 nm LED irradiation change slightly (Fig. 6B). For comparation, the tumor sizes of the mice in other groups (including PBS, DNA-Au/PLNP (light-), DNA-Au/PLNP (light+), TCPP-GDNA-Au/PLNP (light-) groups) obviously increased, indicating the effective inhibiting of tumor growth with the injection of TCPP-GDNA-Au/PLNP after irradiation. The weight of the mice in five groups during treatment did not change significantly (Fig. 6C), suggesting that the nanoparticles in five groups have negligible systemic toxicity and no adverse effects on the body weight following PDT treatment. Moreover, the photographs of the tumor-bearing mice and the excised tumors of respective mice show that the tumor-bearing mouse treated with TCPP-GDNA-Au/PLNP after 650 nm LED irradiation had the smallest tumor size in all groups of mice studied (Fig. S15). The above results indicate that TCPP-GDNA-Au/PLNP dramatically inhibited the growth of the tumor. Hematoxylin and eosin (H&E) staining was also performed to evaluate the PDT treatment efficacy on the tumors. Microscopy images of H&E stained tumor slices reveal serious damage of the tumor cells by the treatment of TCPP-GDNA-Au/PLNP-mediated PDT under 650 nm LED light (Fig. 6D). All above results proved the good efficacy of TCPP-GDNA-Au/PLNP for cancer PDT.

4. Conclusion

We have reported a novel theranostic nanoprobe TCPP-GDNA-Au/PLNP for persistent luminescence imaging-guided PDT. The AS1411 aptamer-contained DNA conjugated Au/PLNP has been rapidly prepared *via* a freezing method without extra reagents giving high content of DNA and good aqueous stability. Meanwhile, TCPP has been easily loaded into the G-quadruplex structure formed from G-rich AS1411 aptamer in the presence of K^+. The nanotheranostic probe gives integrated merits of PLNP for autofluorescence-free bioimging, TCPP for PDT and AS1411 aptamer-contained DNA for specific binding to the over-expressed nucleolin of cancer cells. This work provides a new specially designed imaging-guided PDT nanoplatform for theranostics.

Declaration of competing interest

The authors declare no competing financial interest.

Acknowledgements

This work was supported by the National Natural Science Foundation of China (No. 21934002, 21804056 and 21804057), and the Natural Science Foundation of Jiangsu Province, China (No. BK20180581 and BK20180584), the National First-class Discipline Program of Food Science and Technology (No. JUFSTR20180301), and Collaborative Innovation Center of Food Safety and Quality Control in Jiangsu Province.

Appendix A. Supplementary data

Supplementary data to this article can be found online at https://doi.org/10.1016/j.talanta.2021.122567.

Credit author statement

Yu-Bin Su: Conceptualization, Investigation, Methodology, Data curation, Writing – original draft. Xu Zhao: Methodology, Investigation. Li-Jian Chen: Methodology, Validation. Hai-Long Qian: Methodology, Investigation. Xiu-Ping Yan: Conceptualization, Supervision, Writing – review & editing, Funding acquisition.

References

[1] J. Dai, Y. Li, Z. Long, R. Jiang, Z. Zhuang, Z. Wang, Z. Zhao, X. Lou, F. Xia, B. Z. Tang, Efficient near-infrared photosensitizer with aggregation-induced emission for imaging guided photodynamic therapy in multiple xenograft tumor models, ACS Nano 14 (2020) 854–866.
[2] F. Gao, W. Zheng, L. Gao, P. Cai, R. Liu, Y. Wang, Q. Yuan, Y. Zhao, X. Gao, Au nanoclusters and photosensitizer dual loaded spatiotemporal controllable liposomal nanocomposites enhance tumor photodynamic therapy effect by inhibiting thioredoxin reductase, Adv. Healthcare Mater. 6 (2017) 1601453.
[3] M. Lan, S. Zhao, W. Liu, C.-S. Lee, W. Zhang, P. Wang, Photosensitizers for photodynamic therapy, Adv. Healthcare Mater. 8 (2019) 1900132.
[4] L.-N. Zhu, B. Wu, D.-M. Kong, Specific recognition and stabilization of monomeric and multimeric G-quadruplexes by cationic porphyrin TMPipEOPP under molecular crowding conditions, Nucleic Acids Res. 41 (2013) 4324–4335.
[5] J. Wang, L. Wang, X. Liu, Z. Liang, S. Song, W. Li, G. Li, C. Fan, A gold nanoparticle-based aptamer target binding readout for ATP assay, Adv. Mater. 19 (2007) 3943–3946.
[6] H. Xing, N.Y. Wong, Y. Xiang, Y. Lu, DNA aptamer functionalized nanomaterials for intracellular analysis, cancer cell imaging and drug delivery, Curr. Opin. Chem. Biol. 16 (2012) 429–435.
[7] Q. Hu, H. Li, L. Wang, H. Gu, C. Fan, DNA nanotechnology-enabled drug delivery systems, Chem. Rev. 119 (2019) 6459–6506.
[8] M. Pan, Q. Jiang, J. Sun, Z. Xu, Y. Zhou, L. Zhang, X. Liu, Programming DNA nanoassembly for enhanced photodynamic therapy, Angew. Chem. Int. Ed. 59 (2020) 1897–1905.
[9] T. Saleh, T. Soudi, S.A. Shojaosadati, Aptamer functionalized curcumin-loaded human serum albumin (HSA) nanoparticles for targeted delivery to HER-2 positive breast cancer cells, Int. J. Biol. Macromol. 130 (2019) 109–116.
[10] S. Burge, G.N. Parkinson, P. Hazel, A.K. Todd, S. Neidle, Quadruplex DNA: sequence, topology and structure, Nucleic Acids Res. 34 (2006) 5402–5415.
[11] H.A. Assi1, M. Garavís, C. González, M.J. Damha, I-motif DNA: structural features and significance to cell biology, Nucleic Acids Res. 46 (2018) 8038–8056.
[12] M. Cheng, Y.-X. Cui, J. Wang, J. Zhang, L.-N. Zhu, D.-M. Kong, G-quadruplex/porphyrin Composite photosensitizer: a facile way to promote absorption redshift and photodynamic therapy efficacy, ACS Appl. Mater. Interfaces 11 (2019) 13158–13167.
[13] J. Hu, M. Liu, C. Zhang, Construction of tetrahedral DNA-quantum dot nanostructure with the integration of multistep förster resonance energy transfer for multiplex enzymes assay, ACS Nano 13 (2019) 7191–7201.
[14] R. Mo, T. Jiang, W. Sun, Z. Gu, ATP-responsive DNA-graphene hybrid nanoaggregates for anticancer drug delivery, Biomaterials 50 (2015) 67–74.
[15] J. Ai, Y. Xu, B. Lou, D. Li, E. Wang, Multifunctional AS1411-functionalized fluorescent gold nanoparticles for targeted cancer cell imaging and efficient photodynamic therapy, Talanta 118 (2014) 54–60.
[16] S. Wu, N. Duan, Z. Wang, H. Wang, Aptamer-functionalized magnetic nanoparticle-based bioassay for the detection of ochratoxin a using upconversion nanoparticles as labels, Analyst 136 (2011) 2306–2314.
[17] S.V. Lale, R.G. Aswathy, A. Aravind, D.S. Kumar, V. Koul, AS1411 aptamer and folic acid functionalized pH-responsive ATRP fabricated pPEGMA-PCL-pPEGMA polymeric nanoparticles for targeted drug delivery in cancer therapy, Biomacromolecules 15 (2014) 1737–1752.
[18] J. Wang, Q. Ma, W. Zheng, H. Liu, C. Yin, F. Wang, X. Chen, Q. Yuan, W. Tan, One-dimensional luminous nanorods featuring tunable persistent luminescence for autofluorescence-free biosensing, ACS Nano 11 (2017) 8185–8191.
[19] Z. Pan, Y.-Y. Lu, F. Liu, Sunlight-activated long-persistent luminescence in the near-infrared from Cr^{3+}-doped zinc Gallogermanates, Nat. Mater. 11 (2012) 58–63.
[20] N. Li, Y. Li, Y. Han, W. Pan, T. Zhang, B. Tang, A highly selective and instantaneous nanoprobe for detection and imaging of ascorbic acid in living cells and in vivo, Anal. Chem. 86 (2014) 3924–3930.
[21] J. Liu, T. Lécuyer, J. Seguin, N. Mignet, D. Scherman, B. Viana, C. Richard, Imaging and therapeutic applications of persistent luminescence nanomaterials, Adv. Drug Deliv. Rev. 138 (2019) 193–210.
[22] Y.-B. Su, X. Zhao, L.-J. Chen, H.-L. Qian, X.-P. Yan, 6-Triphenylphosphinehexanoic acid conjugated near-infrared persistent luminescence nanoprobe for autofluorescence-free targeted imaging of mitochondria in cancer cells, ChemNanoMat 6 (2020) 427–434.
[23] T. Maldiney, A. Bessière, J. Seguin, E. Teston, S.K. Sharma, B. Viana, A.J.J. Bos, P. Dorenbos, M. Bessodes, D. Gourier, D. Scherman, C. Richard, The in vivo activation of persistent nanophosphors for optical imaging of vascularization, tumours and grafted cells, Nat. Mater. 13 (2014) 418–426.
[24] Z. Li, Y. Zhang, X. Wu, L. Huang, D. Li, W. Fan, G. Han, Direct aqueous-phase synthesis of sub-10 nm "luminous pearls"with enhanced in vivo renewable near-infrared persistent luminescence, J. Am. Chem. Soc. 137 (2015) 5304–5307.
[25] A. Abdukayum, J.-T. Chen, Q. Zhao, X.-P. Yan, Functional near infrared-emitting Cr^{3+}/Pr^{3+} co-doped zinc gallogermanate persistent luminescent nanoparticles with superlong afterglow for in vivo targeted bioimaging, J. Am. Chem. Soc. 135 (2013) 14125–14133.
[26] T. Maldiney, M. Rémond, M. Bessodes, D. Scherman, C. Richard, Controlling aminosilane layer thickness to extend the plasma half-life of stealth persistent luminescence nanoparticles in vivo, J. Mater. Chem. B. 3 (2015) 4009–4016.
[27] J.-M. Liu, Y.-Y. Liu, D.-D. Zhang, G.-Z. Fang, S. Wang, Synthesis of $GdAlO_3:Mn^{4+}$, Ge^{4+}@Au core-shell nanoprobes with plasmon-enhanced near-infrared persistent luminescence for in vivo trimodality bioimaging, ACS Appl. Mater. Interfaces 8 (2016) 29939.

[28] H.-J. Zhang, X. Zhao, L.-J. Chen, C.-X. Yang, X.-P. Yan, Dendrimer grafted persistent luminescent nanoplatform for aptamer guided tumor imaging and acid-responsive drug delivery, Talanta 219 (2020) 121209.
[29] S.-Q. Wu, C.-X. Yang, X.-P. Yan, A dual-functional persistently luminescent nanocomposite enables engineering of mesenchymal stem cells for homing and gene therapy of glioblastoma, Adv. Funct. Mater. 27 (2017) 1604992.
[30] F. Feng, X. Chen, G. Li, S. Liang, Z. Hong, H.-F. Wang, Afterglow resonance energy transfer inhibition for fibroblast activation protein-α assay, ACS Sens. 3 (2018) 1846–1854.
[31] W. Wu, Q. He, H. Chen, J. Tang, L. Nie, Sonochemical synthesis, structure and magnetic properties of air-stable Fe_3O_4/Au Nanoparticles, Nanotechnology 18 (2007) 145609.
[32] B. Liu, J. Liu, Freezing directed construction of bio/nano interfaces: reagentless conjugation, denser spherical nucleic acids, and better nanoflares, J. Am. Chem. Soc. 139 (2017) 9471–9474.
[33] Y.-J. Li, X.-P. Yan, Synthesis of functionalized triple-doped zinc gallogermanate nanoparticles with superlong near-infrared persistent luminescence for long-term orally administrated bioimaging, Nanoscale 8 (2016) 14965–14970.
[34] X. Zhao, K.-C. Zhao, L.-J. Chen, Y.-S. Liu, J.-L. Liu, X.-P. Yan, A pH reversibly activatable NIR photothermal/photodynamic-in-one agent integrated with renewable nanoimplants for image-guided precision phototherapy, Chem. Sci. 12 (2021) 442–452.
[35] X. Li, C. Weng, J. Wang, W. Yang, Q. Lu, X. Yan, M.A. Sakran, J. Hong, W. Zhu, X. Zhou, A label-free electrochemical magnetic aptasensor based on exonuclease III-assisted signal amplification for determination of carcinoembryonic antigen, Microchim Acta 187 (2020) 492.
[36] M.A. Abedalwafa, Z. Tang, Y. Qiao, Q. Mei, G. Yang, Y. Li, L. Wang, An aptasensor strip-based colorimetric determination method for kanamycin using cellulose acetate nanofibers decorated DNA-gold nanoparticle bioconjugates, Microchim Acta 187 (2020) 360.
[37] L. Riauba, G. Niaura, O. Eicher-Lorka, E. Butkus, A study of cysteamine ionization in solution by Raman spectroscopy and theoretical modeling, J. Phys. Chem. 110 (2006) 13394–13404.
[38] B. Shi, Y. Su, L. Zhang, R. Liu, M. Huang, S. Zhao, Nitrogen-rich functional groups carbon nanoparticles based fluorescent pH sensor with broad-range responding for environmental and live cells applications, Biosens, Bioelectron 82 (2016) 233–239.
[39] S.J. Hurst, A.K.R. Lytton-Jean, C.A. Mirkin, Maximizing DNA loading on a range of gold nanoparticle sizes, Anal. Chem. 78 (2006) 8313–8318.
[40] X. Zhang, M.R. Servos, J. Liu, Instantaneous and quantitative functionalization of gold nanoparticles with thiolated DNA using a pH-assisted and surfactant-free route, J. Am. Chem. Soc. 134 (2012) 7266–7269.
[41] Y. Miao, S. Lv, D. Zheng, Y. Liu, D. Liu, F. Song, Porphyrin-based metal coordination polymers with self-assembly pathway-dependent properties for photodynamic and photothermal therapy, Biomater. Sci. 9 (2021) 2533–2541.
[42] W. Pang, P. Jiang, S. Ding, Z. Bao, N. Wang, H. Wang, J. Qu, D. Wang, B. Gu, X. Wei, Nucleolus-targeted photodynamic anticancer therapy using renal-clearable carbon dots, Adv. Healthcare Mater. 9 (2020) 2000607.
[43] Z. Cai, F. Xin, Z. Wei, M. Wu, X. Lin, X. Du, G. Chen, D. Zhang, Z. Zhang, X. Liu, C. Yao, Photodynamic therapy combined with antihypoxic signaling and CpG adjuvant as an in situ tumor vaccine based on metal-organic framework nanoparticles to boost cancer immunotherapy, Adv. Healthcare Mater. 9 (2020) 1900996.